

# Electrodeposition of Ultrathin Nanosheets of Nickel-Cobalt Double Hydroxides with Layered Structure for Improved Supercapacitor Performance

Ao Ju<sup>2</sup>, Ruidong Xu<sup>1,2,\*</sup>, Ying Zhang<sup>2</sup>, Suyang Feng<sup>1,2</sup>, Chen Chen<sup>2</sup>, Jiang Liao<sup>1,2</sup>

<sup>1</sup> State Key Laboratory of Complex Nonferrous Metal Resources Clean Utilization, Kunming University of Science and Technology, Kunming 650093, China

<sup>2</sup> Faculty of Metallurgical and Energy Engineering, Kunming University of Science and Technology, Kunming 650093, China

\*E-mail: [rdxupaper@aliyun.com](mailto:rdxupaper@aliyun.com)

Received: 10 December 2020 / Accepted: 19 January 2021 / Published: 28 February 2021

Ultrathin nanosheet structures of tremella-like nickel-cobalt layered double hydroxide (LDH) grown on nickel foam were successfully prepared by a simple procedure involving the electrodeposition method. The obtained nickel foam supported tremella-like nickel-cobalt LDH nanosheet material can be directly used as a supercapacitor electrode. FE-SEM, Raman spectroscopy, XRD, and XPS were used to examine the microstructure, molecular bond energy structure, phase structure, and valence state of the material, and its electrochemical properties were tested by CV, GCD, and EIS. By adjusting the  $\text{NiCl}_2/\text{Co}(\text{NO}_3)_2$  mole ratios in the electrodeposition electrolyte, the sample morphology and electrochemical properties can be controlled. When the Ni/Co molar ratio was 2/1 under the optimal deposition conditions, the sample demonstrated high specific capacitances of  $2065 \text{ F}\cdot\text{g}^{-1}$  and  $2357.5 \text{ F}\cdot\text{g}^{-1}$  at current densities of  $10 \text{ A}\cdot\text{g}^{-1}$  and  $1 \text{ A}\cdot\text{g}^{-1}$ , indicating good rate capability. After charging and discharging for 3000 cycles at  $10 \text{ A}\cdot\text{g}^{-1}$  in 2 M KOH, the capacitance remains 81.8%, exhibiting superior recycling stability. The outstanding electrochemical performance of the electrode is mainly attributed to the ultrathin nanosheets, the excellent redox reversibility, and the synergistic effects between  $\text{Ni}(\text{OH})_2$  and  $\text{Co}(\text{OH})_2$ . Therefore, this remarkable new electrode material has promising applications in electrochemical energy storage.

**Keywords:** Ni-Co layered double hydroxides, electrodeposition, specific capacity, cyclic stability, supercapacitors

## 1. INTRODUCTION

A series of energy problems caused by the overexploitation of nonrenewable energy are some of the most critical social issues that humans have faced since industrialization began [1, 2]. There is an

urgent need for clean, nonpolluting, sustainable energy and new technologies related to energy conversion and storage [3]. Supercapacitors are characterized by safety and stability, high capacitance, high power density, fast charging and discharging, long life, and environmental protection [4]. They are now high-performance energy storage devices with enormous growth and market potential [5, 6]. Many researchers in materials science, manufacturing technology, and so on continue to promote technological progress to improve the performance of supercapacitors to overcome their shortcomings and enable greater application value [7, 8].

At present, according to the difference in the energy storage mechanism, supercapacitors can be divided into two types: electric double-layer capacitors and pseudocapacitors [9, 10]. The energy storage capacity of electric double-layer capacitors is still low, which fundamentally limits their application prospects as major energy storage devices. The advantage of the pseudocapacitor energy storage mechanism is that, through the Faraday reaction, not only the surface of the electrode material but also the internal electrode material can participate in energy storage so that a higher specific capacity and energy density can be obtained [11]. The electrode materials of pseudocapacitors are mainly composed of conductive polymers, and transition metal hydroxides or oxides, and transition metal hydroxides have been widely studied due to their high theoretical specific capacitance value and unique redox effect [12].

Notably, several recent studies have shown that  $\text{Ni(OH)}_2$  deposited directly on three-dimensional (3D) nickel foam has a high specific capacitance [13]. However, the loading capacity of  $\text{Ni(OH)}_2$  is limited. Considering the effect of  $\text{Co(OH)}_2$  on the electrochemical performance of  $\text{Ni(OH)}_2$  electrodes in supercapacitors, the construction of  $\text{Co(OH)}_2/\text{Ni(OH)}_2$  composite electrodes for pseudocapacitors is a good choice [14]. In recent years, researchers have conducted in-depth studies on Ni-Co LDHs, which are characterized by low cost, good electrical conductivity, and nontoxicity [15]. These characteristics make it more electrochemical than a single nickel or cobalt hydroxide [16, 17]. In addition, nickel foam has redox activity in alkaline electrolytes, which may exaggerate the observed results [18]. In the most recent literature, Li et al. synthesized 3D flower-like Ni-Co double hydroxide (Ni-Co DH) microspheres by microwave irradiation. The specific capacitance of the Ni-Co DH electrode at  $1 \text{ A}\cdot\text{g}^{-1}$  is  $1120 \text{ F}\cdot\text{g}^{-1}$ . After 1000 cycles at  $30 \text{ A}\cdot\text{g}^{-1}$ , the capacitance value remained at 93.8% [19]. Ma and his colleagues prepared cobalt and iron hydroxides on  $\text{NiO}$  by chemical bath deposition, and the specific capacity of the prepared electrode was  $361 \text{ C}\cdot\text{g}^{-1}$  at  $1 \text{ A}\cdot\text{g}^{-1}$  [20]. Gao et al. reported a promising material, Ni-Co layered hydroxides, synthesized by simple hydrothermal coprecipitation. When the current density is  $4 \text{ mA}\cdot\text{cm}^{-2}$ , the capacitance of the material is  $6.368 \text{ F}\cdot\text{cm}^{-2}$ . After 2000 cycles, the original capacitance is still 79.9% [21]. Compared with the above methods, the preparation of Ni-Co LDHs by the electrodeposition method is simple and direct. Electrodeposition has the advantages of a short reaction time, mild reaction temperature, and good controllability.

In this article, Ni-Co LDH electrode materials were prepared by constant voltage electrodeposition on the surface of a nickel foam matrix. Herein, Ni-Co LDHs of ultrathin nanosheets were obtained using a mixture of cobalt nitrate and nickel chloride as an electrolyte. By changing the molar ratio of the two precursors, the ultrathin Ni-Co LDH nanostructures could be controlled, resulting in changes in electrochemical properties. The electrochemical properties, such as the cyclic voltammetry curve, constant current charge-discharge curve, AC impedance spectrum, and physical properties, such as the surface morphology and phase composition of the electrode materials were tested. Ni-Co LDHs

on nickel foam substrates have a high specific capacity and excellent capacitance retention. The excellent electrochemical performance and cyclic stability of the prepared material are mainly attributed to the sheet nanostructure, the synergistic effect of pseudocapacitive materials and the excellent reversibility.

## 2. EXPERIMENTAL

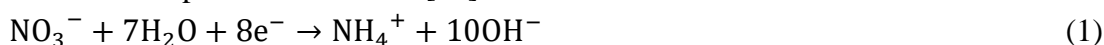
### 2.1 Matrix pretreatment

After cutting the nickel foam (NF) into a sheet with an area of 10×20 mm, to remove the surface oxide, it was immersed in 3 mol/L hydrochloric acid and put into an ultrasonic cleaning apparatus for cleaning. After 30 minutes, the NF was removed, and it was ultrasonically cleaned with anhydrous ethanol and deionized water to obtain pure NF. The samples were placed in a vacuum drying oven and dried for later use.

### 2.2 Preparation of Ni-Co LDH nanosheets

Nickel chloride ( $\text{NiCl}_2 \cdot 6\text{H}_2\text{O}$ ) and cobalt nitrate ( $\text{Co}(\text{NO}_3)_2 \cdot 6\text{H}_2\text{O}$ , 5 mM) were placed in 60 ml deionized water, and the electrolyte was placed in a constant temperature magnetic stirring water bath at 25°C and stirred for 20 minutes until completely dissolved to obtain a clear solution. When the molality ratios of nickel chloride and cobalt nitrate were 1:1, 2:1, 3:1, 4:1, and 5:1, the prepared samples were recorded as NC-1, NC-2, NC-3, NC-4, and NC-5, respectively.

In this experiment, the PARSTAT2273 electrochemical workstation was mainly used. NF pretreated by the working electrode, reference charge extremely saturated calomel electrode (SCE), and platinum electrode for the auxiliary electrode. Three electrodes were placed into the configured electrolyte, and electrodeposition was performed using the constant pressure method. The deposition potential is -0.95 V, and the deposition time is 300 s. The electrodeposition process of the Ni-Co LDH nanosheets can be expressed as follows [22]:



After electrodeposition, the prepared samples were carefully cleaned with deionized water and then dried in a 60 °C drying oven for 3 hours. After drying, the mass of the deposited active substance was the total weight of the sample minus the mass of the NF, which was approximately 1.3 mg/cm<sup>2</sup>. The deposition of Ni-Co LDH on the NF substrate was performed via electrodeposition, as shown in Fig. 1.

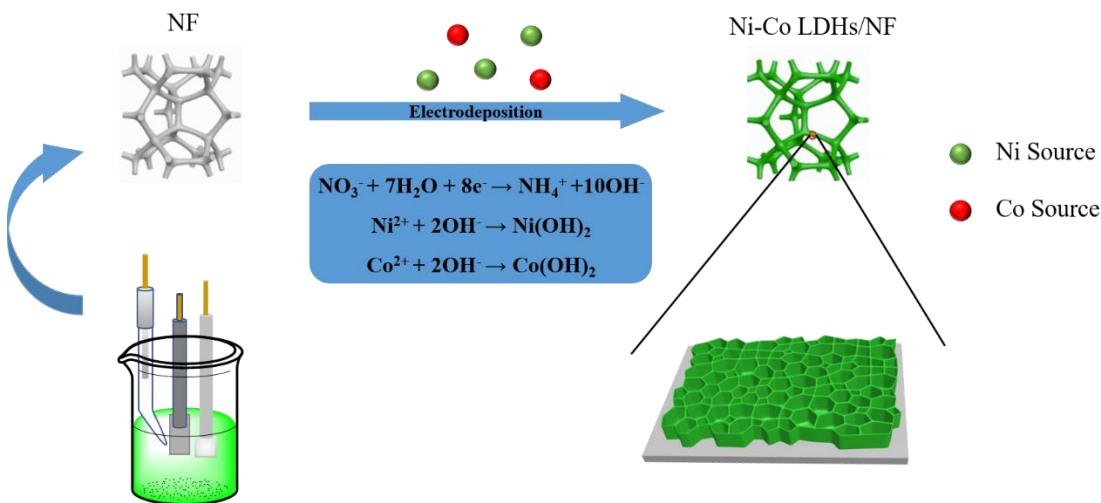


**Figure 1.** Schematic diagram of synthesis of Ni-Co LDHs nanomaterials on NF.

#### 2.4 Characterization

The surface morphology and elemental composition of the deposited samples were characterized by field emission scanning electron microscopy (SEM, Nove NanoSEM 450) with a 15 kV energy dispersive X-ray (EDS) system. Raman spectra were acquired with a DXRxi-Raman spectrometer (Madison WI 537711, America) under an excitation wavelength of 532 nm. The X-ray diffraction pattern (XRD) of the electrode material was obtained by using a D/Max 2200 X-ray diffractometer (XRD, Cu K $\alpha$  radiation). X-ray photoelectron spectroscopy (XPS) was used to analyze the chemical structure and composition of the deposited samples on a PHI 5500 X-ray photoelectron spectroscope.

#### 2.5 Electrochemical measurements

Measurements of electrochemical performance included cyclic voltammetry (CV), galvanostatic charge-discharge (GCD), electrochemical impedance spectroscopy (EIS), and cyclic stability. All measurements were made at 25 °C with a CHI760D electrochemical workstation using a three-electrode system and 60 ml electrolyte (2 M KOH). In this experiment, a saturated calomel electrode (SCE) was used as the reference electrode, and a platinum column was used as the counter electrode; the working electrode was Ni-Co LDH nanosheets on NF substrates. The specific capacitance can be calculated from the discharge curves according to the following formula [23]:

$$C = (I \cdot \Delta t) / (m \cdot \Delta V) \quad (4)$$

where C represents the specific capacitance value ( $F \cdot g^{-1}$ ); I is the discharge current (A);  $\Delta t$  is the discharge time (s); m is the quality of the active substance (g); and  $\Delta V$  is the voltage range (V).

### 3. RESULTS AND DISCUSSION

#### 3.1 Phase structures and microstructural analysis

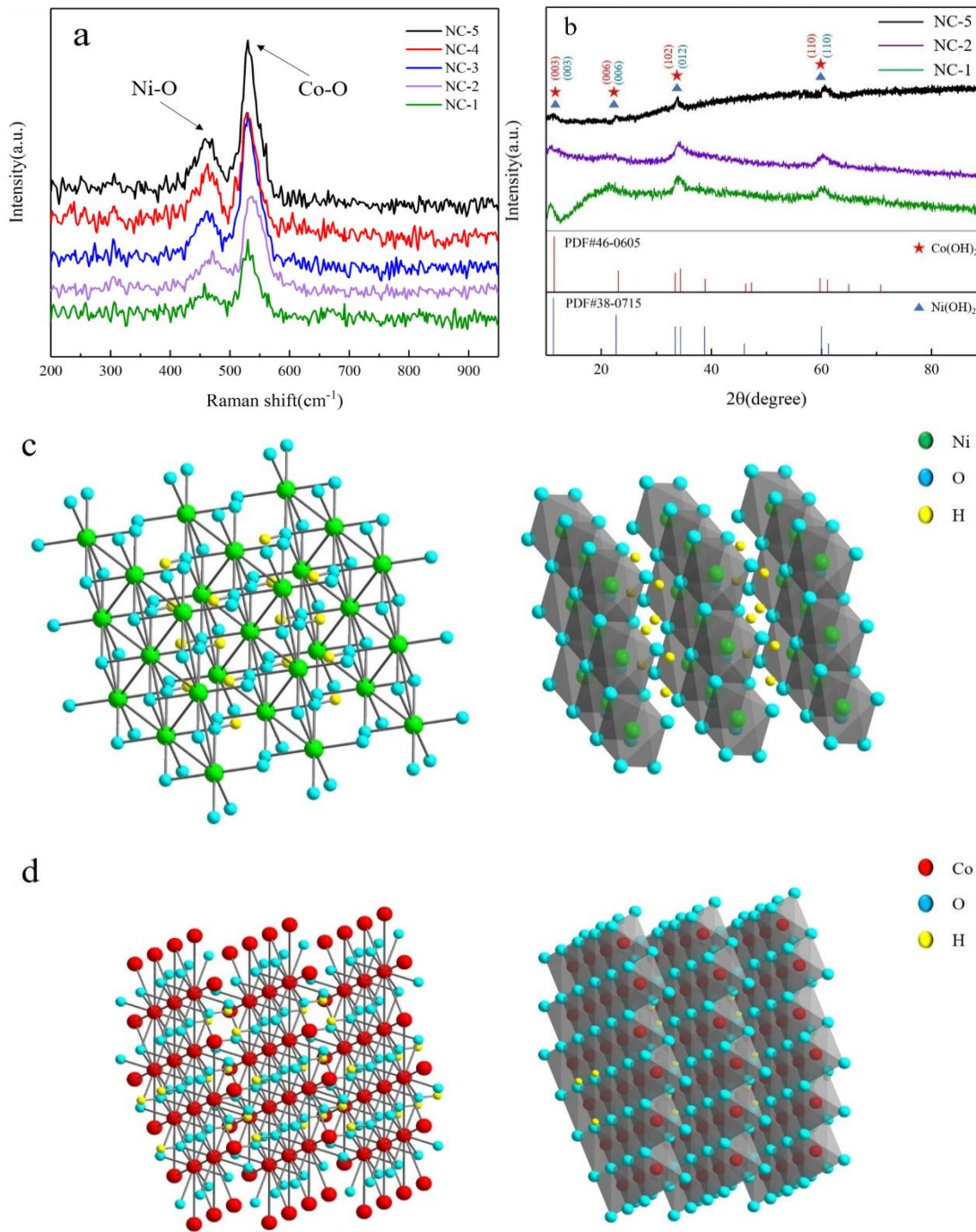


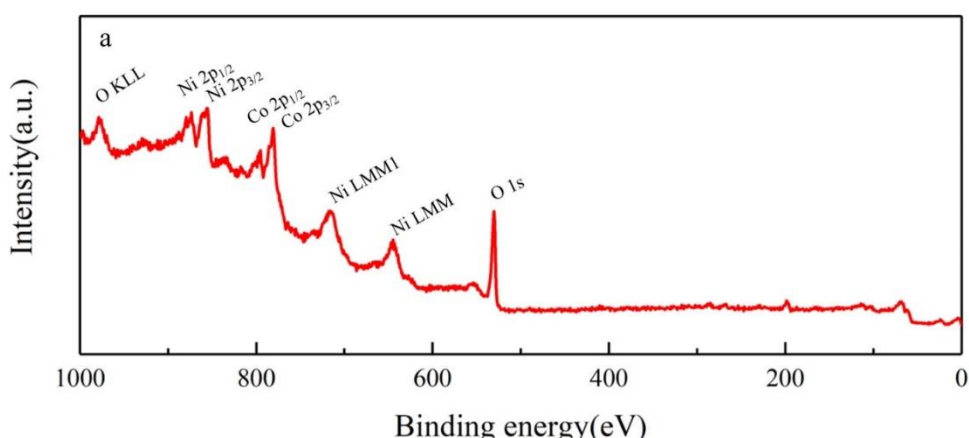
**Figure 2.** Spectroscopy analyses of amorphous Ni-Co LDHs materials. (a) Raman spectra, (b) XRD patterns, (c) the crystal structure of  $\text{Ni(OH)}_2$  in ball-and-stick model and in polyhedral model and (d) the crystal structure of  $\text{Co(OH)}_2$  in ball-and-stick model and in polyhedral model.

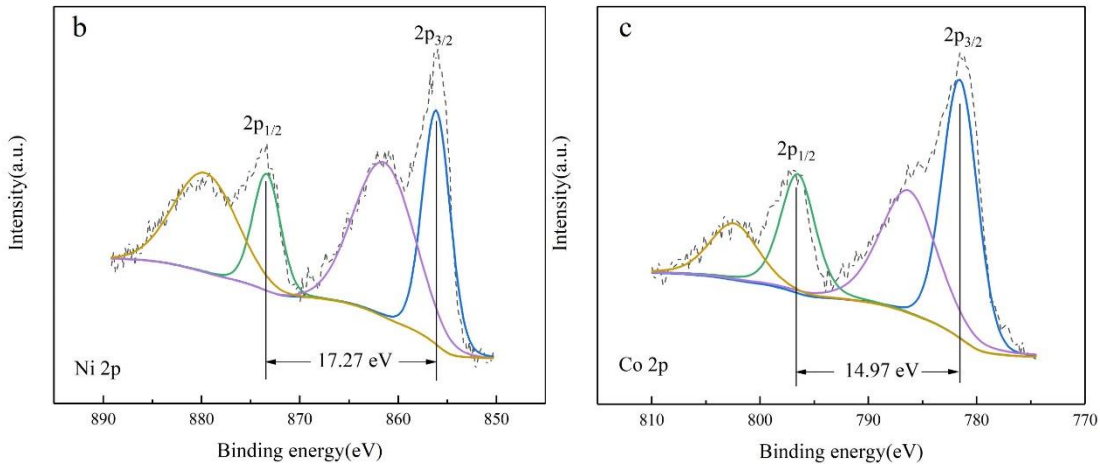
To determine the structure of Ni-Co LDHs, the samples were characterized by Raman spectra and XRD, and the test results are shown in Fig. 2. The Raman test results of Ni-Co LDHs (Fig. 2a)

showed that Ni-O and Co-O vibration peaks appeared at 450 and 520 cm<sup>-1</sup>, respectively, indicating the existence of Ni-O and Co-O bonds in the material, which further confirmed that the prepared materials were Ni(OH)<sub>2</sub> and Co(OH)<sub>2</sub> [24, 25].

X-ray diffraction analysis was used to determine the phase of the prepared Ni-Co LDHs, and the results are shown in Fig. 2(b). This figure contains the X-ray diffraction patterns of 3 samples prepared under different Ni/Co ratios in electrolyte conditions. During the XRD test, the active substance is separated from the nickel foam matrix with a clean knife. Due to the weak crystallinity of the materials synthesized at room temperature, the strength of the diffraction peak is relatively weak. In addition, there are defects in the weak crystal material, which is conducive to the electrochemical measurement of redox reaction electrons and ion transfer, thus improving the electrochemical performance of electrode materials [26]. Some obvious diffraction peaks can be seen at the positions with values of 11.3°, 22.7°, 34.4°, and 59.9°, which are close to (0 0 3), (0 0 6), (0 1 2), and (1 1 0) of the standard spectrum of Ni(OH)<sub>2</sub> (PDF#38-0715) by comparison [27]. The peaks at 11.5°, 23.2°, 34.4°, and 59.8° can be assigned to the (0 0 3), (0 0 6), (1 0 2), and (1 1 0) reflections of Co(OH)<sub>2</sub> (PDF#46-0605) respectively [28]. It is not easy to distinguish between the two phases because they have similar structures and their diffraction peaks are very close together. The expansion of the (0 0 3) and (1 1 0) peaks of the material can be observed, showing the joint action of Ni(OH)<sub>2</sub> and Co(OH)<sub>2</sub> [29].

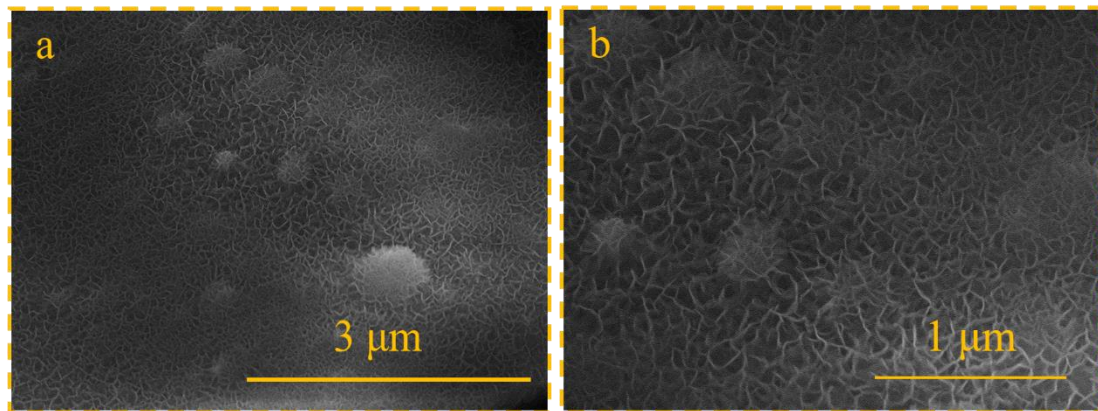
Fig. 2(c-d) displays the crystal structures of Ni(OH)<sub>2</sub> and Co(OH)<sub>2</sub> in the ball-and-stick model and in the polyhedral model. Fig. 2(c) shows that Ni(OH)<sub>2</sub> crystallizes in the trigonal P-3m1 space group. The structure is two-dimensional and consists of one Ni(OH)<sub>2</sub> sheet oriented in the (0, 0, 1) direction. Ni(1) is bonded to six equivalent O(1) atoms. The edge lengths of the unit cell, namely, the lattice constants *a*, *b* and *c*, are 3.165 Å, 3.165 Å, and 9.354 Å, respectively, and *a*=*b*≠*c*. The angles  $\alpha$ ,  $\beta$ , and  $\gamma$  between the edges of the unit cell are 90.492°, 90.492°, and 60.037°,  $\alpha=\beta\neq\gamma$ . Hence, the Ni(OH)<sub>2</sub> crystallizes in the rhombohedral system. Fig. 2(d) shows that Co(OH)<sub>2</sub> crystallizes in the trigonal P-3m1 space group. The structure is two-dimensional and consists of one Co(OH)<sub>2</sub> sheet oriented in the (0, 0, 1) direction. Co(1) is bonded to six equivalent O(1) atoms to form edge-sharing CoO<sub>6</sub> octahedra. The *a* is 3.209 Å, the *b* is 3.225 Å, and the *c* is 4.779 Å. So, *a*≠*b*≠*c*. The  $\alpha$  is 90.715°,  $\beta$  is 89.900° and  $\gamma$  is 120.449°,  $\alpha\neq\beta\neq\gamma$ . Therefore, Co(OH)<sub>2</sub> crystallization is a simple triclinic system. These crystal structures can provide more active sites for reactivity, which makes the redox reaction of electrode materials more complete when conducting electrochemical performance tests.





**Figure 3.** (a) XPS spectra of NC-2/NF, (b-c) Ni 2p, Co 2p XPS spectra of NC-2/NF.

XPS analysis test proved the existence of Ni, Co, and valence states of elements. The results are shown in Fig. 3(a–c). The survey spectrum (Fig. 3a) indicates the presence of Co, Ni, and O elements in Ni-Co LDH/NF. The high-resolution energy spectrum of Ni 2p is shown in Fig. 3(b); the peaks at 856.28 eV and 873.55 eV are attributed to Ni 2p<sub>3/2</sub> and Ni 2p<sub>1/2</sub> separated from the Ni 2p region. It can also be seen that the difference in the binding energy between the Ni 2p<sub>3/2</sub> edge and Ni 2p<sub>1/2</sub> is 17.27 eV, which is characteristic of Ni<sup>2+</sup>, suggesting the existence of Ni(OH)<sub>2</sub> [30]. In the high-resolution energy spectrum of Co 2p, in Fig. 3(c), there are two major peaks at binding energies of 781.79 and 786.03 eV, corresponding to the spin orbitals of Co2p<sub>3/2</sub> and Co 2p<sub>1/2</sub>, and the difference value of their binding energy is 14.97 eV, indicating the existence of bivalent Co<sup>2+</sup> in Co(OH)<sub>2</sub> [31]. Obviously, Ni(OH)<sub>2</sub> and Co(OH)<sub>2</sub> components coexist in the Ni-Co LDHs. In addition, there are no other elements present in XRD and XPS. Therefore, it can be inferred that Ni-Co double hydroxide nanomaterials have been synthesized.



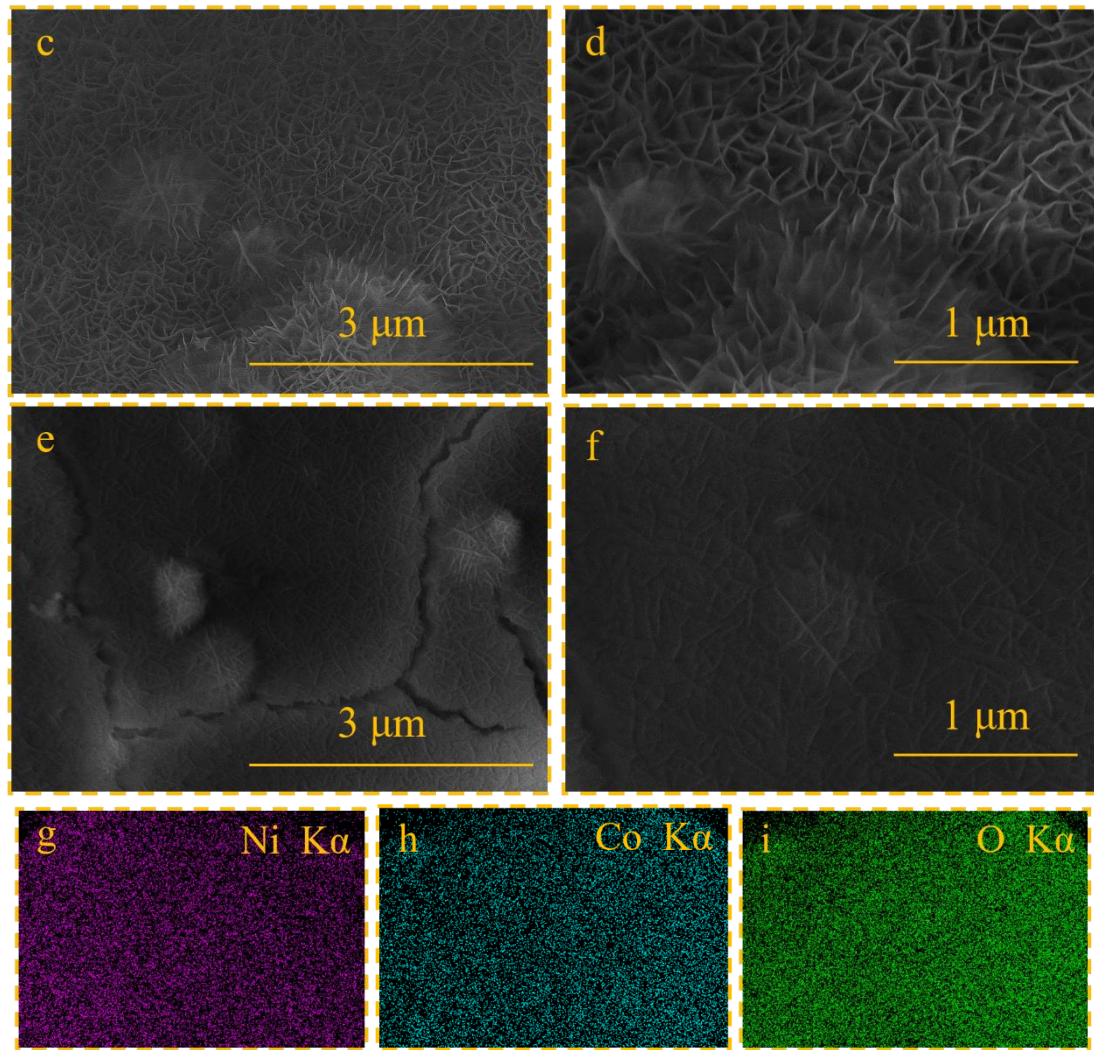


**Figure 4.** FE-SEM images of the Ni-Co LDHs nanosheets on NF: (a and b) NC-1, (c and d) NC-2, (e and f) NC-5 and (g)-(i) showing elemental mappings for Ni, Co, and O of image (b).

The FE-SEM images of NC-1, NC-2 and NC-5 on NF substrates are shown in Fig. 4(a-f). As shown in Fig. 4(a), the entire surface of the nickel foam matrix is uniformly covered by a microscopic network structure. The associated high-magnification SEM image (Fig. 4b) clearly shows that the network is composed of many interlaced nanosheets. In addition, some small aggregates composed of nanosheets appeared on the surface of the network structure. With the increase in  $\text{Ni}^{2+}$  content in the sample, as shown in Fig. 4(c-d), the aggregate shape becomes a tremella-like structure, with more obvious folds. The specific surface area of the nanosheet increases, providing more active sites, a more complete redox reaction, and better electrochemical performance [32]. For NC-5/NF, in Fig. 4(e-f), the surface morphology has many cracks and small particles, which may be caused by the reduction in  $\text{OH}^-$ . According to Eqs. (1), the proportion of  $\text{Co}(\text{NO}_3)_2$  in the electrolyte decreases, and the content of  $\text{NO}_3^-$  decreases, leading to a decrease of  $\text{OH}^-$ . Through EDS elemental mapping analysis of the NC-1/NF sample, the elemental distribution diagram of Ni, Co, and O is shown in Fig. 4(g-i). The three elements are uniformly distributed over the entire surface of the sample.

### 3.2 Electrochemical properties

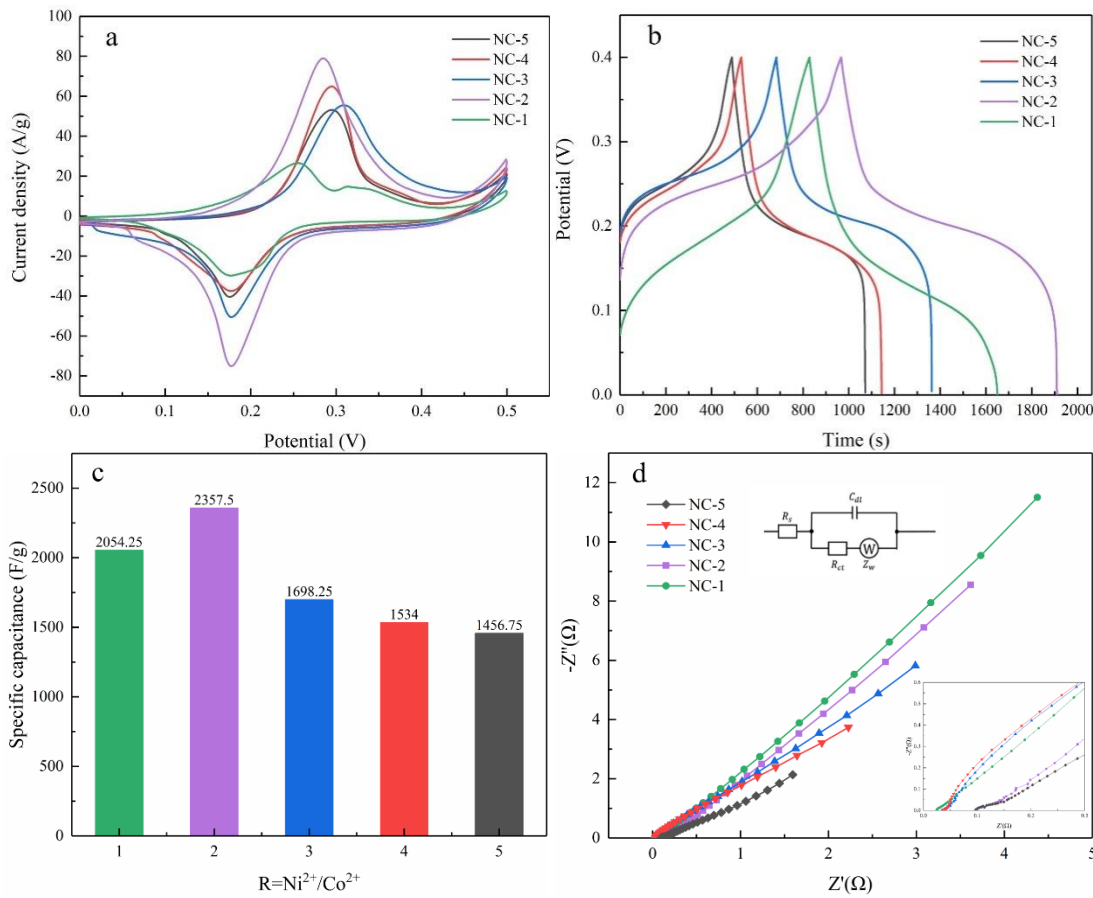
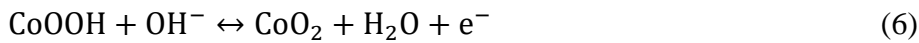


**Figure 5.** Comparison of electrochemical properties of 5 samples: (a) CV curves at a scan rate  $10 \text{ mV}\cdot\text{s}^{-1}$ , (b) GCD curves at a current density of  $1 \text{ A}\cdot\text{g}^{-1}$ , (c) the specific capacity of the Ni-Co LDHs of R at a current density of  $1 \text{ A}\cdot\text{g}^{-1}$ , and (d) the Nyquist plots of the Ni-Co LDHs with different Ni/Co ratios in three-electrode system. Inset: the zoom-in Nyquist plots at the high-frequency region and the equivalent circuit diagram.

Fig. 5(a) shows a comparison of the CV curves of Ni-Co LDH materials at different Ni/Co synthesis ratios ( $R = 1:1, 2:1, 3:1, 4:1, 5:1$ ) at a scanning rate of  $10 \text{ mV}\cdot\text{s}^{-1}$  and over a voltage range of 0 to  $0.5\text{V}$ . There are apparent strong redox peaks in all the samples tested, which indicates that the samples we prepared have good pseudocapacitance behavior. In KOH solution, the redox reaction of  $\text{Co(OH)}_2$  and  $\text{Ni(OH)}_2$  in the active substance on NF can be expressed as [29, 33]:



From the reaction equations, it can be concluded that the oxidation peak of high voltage corresponds to the oxidation reaction of the Ni phase, and the peak of low potential is the Co phase. Two almost overlapping redox peaks widened the redox characteristics and improved the redox reaction. The area enclosed by the CV curve represents the capacitance of the electrode material. It can be clearly seen from the figure that the area enclosed by the CV curve under the composite ratio of  $R = 2:1$  is the largest,

indicating that the sample has the maximum specific capacitance under this ratio. The GCD curves in Fig. 5(b) also verify the conclusion of the CV curve test. The length of the right half of the GCD curve indicates the duration of the discharge time during the reduction process, and the discharge time of sample NC-2 is the longest. Fig. 5(c) shows the specific capacitance change curve of samples with different synthesis ratios  $R$  ( $=\text{Ni}^{2+}/\text{Co}^{2+}$ ) under the condition of a current density of  $1 \text{ A}\cdot\text{g}^{-1}$ . When the Ni/Co molar ratios were 1:1, 2:1, 3:1, 4:1, and 5:1, the specific capacitance results of the corresponding samples were 2054.25, 2357.5, 1698.25, 1534, and  $1456.75 \text{ F}\cdot\text{g}^{-1}$ , respectively. As seen from the curve change, in the electrolyte within a certain concentration range, with increasing Ni content, the specific capacitance of the sample first increases and then decreases. In other words, an appropriate amount of Ni can promote an increase in electrode material-specific capacitance in supercapacitors. However, when the nickel content is too high, the specific capacitance value will decrease. When the synthetic ratio  $R=2:1$ , the specific capacitance of the Ni-Co LDH/NF material was the highest, which also corresponded well to the morphological analysis results.

Further impedance analysis of Ni-Co LDH/NF electrode materials was performed using EIS tests at frequencies ranging from 10 kHz to 100 MHz. Fig. 5(d) shows Nyquist plots of Ni-Co LDH/NF electrode materials, where  $Z'$  and  $-Z''$  are the real and imaginary parts of the impedance, respectively. The whole curve can be divided into two parts: the high-frequency region (a semicircle) and the low-frequency region (a straight line). The numerical value of the position where the semicircular arc intersects the real axis in the high-frequency region can be regarded as the internal resistance ( $R_s$ ) of the electrode, which includes the ionic resistance of the electrolyte, the intrinsic resistance of the active substance, and the contact resistance between the active substance and the matrix [34].

**Table 1.** Parameter values of different Ni-Co LDHs/NF electrodes obtained by equivalent circuit simulation

Samples	$R_s/\Omega$	$C/\text{F}$	$R_{ct}/\Omega$	$Z_w/\Omega$
NC-1	0.097	0.0325	0.1186	0.0903
NC-2	0.025	0.0326	0.0017	0.1368
NC-3	0.039	0.1216	2.3600	0.0884
NC-4	0.035	0.1029	1.6037	0.2307
NC-5	0.096	0.3409	1.4580	0.2197

According to Fig. 5(d) shown in the illustration of the equivalent circuit diagram, through the fitting analysis, the specific results are shown in Table 1. The  $R_s$  values of NC-1, NC-2, NC-3, NC-4, and NC-5 were  $0.097 \Omega$ ,  $0.025 \Omega$ ,  $0.039 \Omega$ ,  $0.035 \Omega$ , and  $0.096 \Omega$ , respectively. The phenomenon of the semicircle in the high-frequency region is due to resistance ( $R_{ct}$ ) caused by the redox reaction on the surface of the charge transfer electrode material [35]. Fig. 5(d) shows that sample NC-2 presents a smaller semicircle at high frequency, and  $R_{ct}$  is  $0.0017 \Omega\cdot\text{cm}^2$ , indicating that the NC-2/NF material electrode has a lower charge transfer resistance, faster charge transfer, and better redox reaction. The straight line of the low-frequency portion of EIS represents the diffusion and migration of ions in the

active substance on the electrode associated with Warburg resistance ( $Z_w$ ). In the illustration, the curve slope of the NC-2 sample is relatively small, indicating that the ion diffusion rate between the electrode and electrolyte is faster. This result is consistent with higher specific capacitance and better rate performance. Therefore, samples under this ratio were selected for further research and analysis.

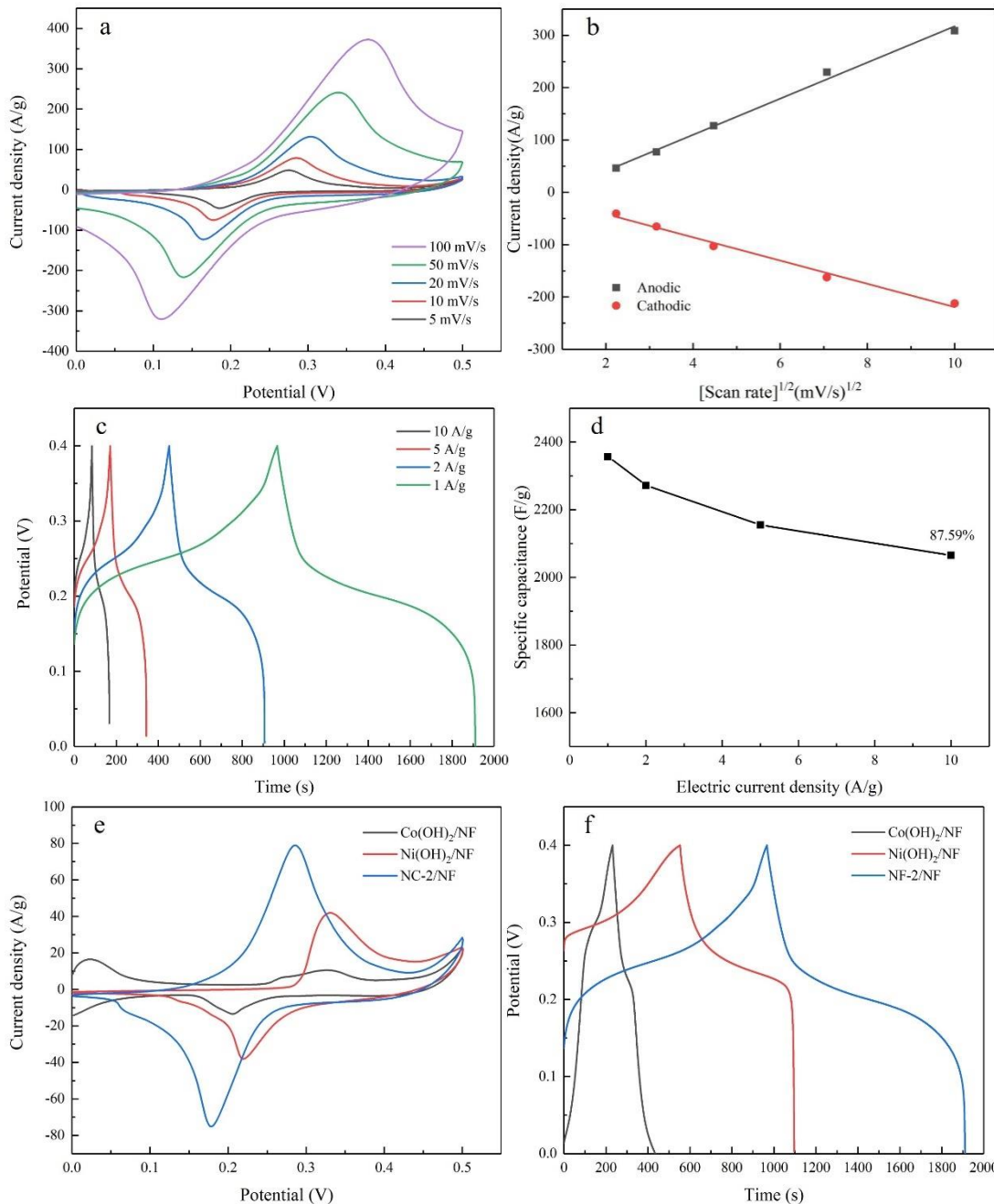


**Figure 6.** Electrochemical properties of NC-2/NF: (a) CV curves at different scanning rates, (b) the linear relationship curve between oxidation peak and reduction peak distribution and the square root of current density, (c) GCD curves at different current densities, (d) specific capacitance change curve at different current densities, (e) CV curves at a scan rate of  $10\text{ mV}\cdot\text{s}^{-1}$ , and (f) GCD curves at a current density of  $1\text{ A}\cdot\text{g}^{-1}$  of NC-2/NF and its unitary hydroxide.

Fig. 6(a) shows the CV curve of sample NC-2/NF at different scanning rates. The redox reactions can be expressed according to Eqs.(5)–(7), as mentioned above. It can be clearly seen that with the acceleration of the scanning rate, the diffusion rate of ions is affected, the current of the redox peak increases gradually, and the oxidation peak and reduction peak move to higher and lower potential directions, respectively. At a scanning rate of  $100 \text{ mV}\cdot\text{s}^{-1}$ , the CV curve maintained a good shape, indicating that the electrode material had good stability and reversibility and showed the potential of the electrode material in energy storage. As shown in Fig. 6(b), is the square root of the reductive peak current and scan rate curve shows a good linear relationship. The whole reaction process is controlled by the spread of  $\text{OH}^-$ , and  $\text{OH}^-$  plays a leading role in a redox reaction, showing that the material has good fast charge transfer capability and good electrical conductivity [36]. Fig. 6(c) shows the constant current charge-discharge curve of the sample. The specific capacitance values at current densities of 1, 2, 5, and  $10 \text{ A}\cdot\text{g}^{-1}$  are 2357.5, 2272.5, 2155, and  $2065 \text{ F}\cdot\text{g}^{-1}$ , respectively, and Fig. 6(d) shows a multiplier performance of 87.59%.

In addition, the electrochemical properties of NC-2/NF and a single hydroxide were compared by the CV curve and GCD curve. As the specific capacitance is positively correlated with the area of the closed CV curve, it can be seen from Fig. 6(e) that the specific capacitance of the experimental sample NC-2/NF is significantly higher than that of  $\text{Ni(OH)}_2$  and  $\text{Co(OH)}_2$ . Fig. 6(f) shows the GCD curve of NC-2/NF and its single hydroxide when the current density is  $1 \text{ A}\cdot\text{g}^{-1}$ . The specific capacity of NC-2/NF is the highest among the three materials, which is conducive to the improvement of electrochemical activity. This result is consistent with the CV curve.

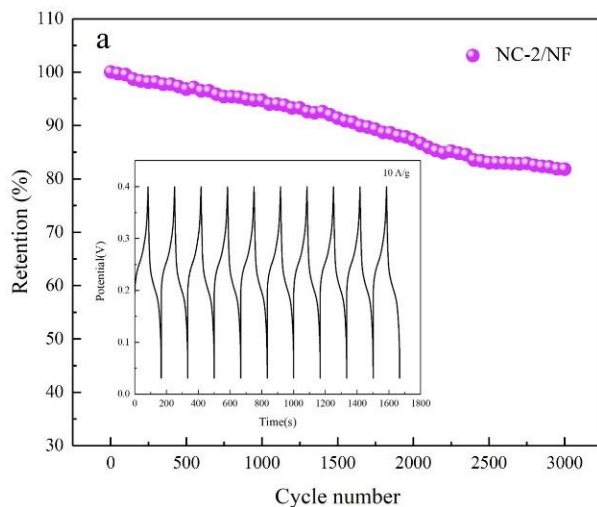


**Figure 7.** (a) Cycling performances of NC-2/NF at a current density of  $10 \text{ A}\cdot\text{g}^{-1}$ .

To prove that appropriate contents of Ni can improve the conductivity of Ni-Co LDH/NF electrode materials, the electrochemical properties of the sample were tested at room temperature. The cycling performance of the NC-2/NF electrode material was measured by GCD under a current density of  $10 \text{ A}\cdot\text{g}^{-1}$  within the potential window of 0 - 0.4 V, as shown in Fig. 7(a). It is obvious that the specific

capacity retention rate of the NC-2/NF material remained at 81.8%, showing good circulation performance after 3000 cycles.

**Table 2.** Comparison of the specific capacity performance of several types of composite materials

Material	Morphology	Method	Specific capacity (F g <sup>-1</sup> )	Capacitance retention (cycles)	Reference
Ni-Co layered double hydroxides	nanosheets	Hydrothermal	1734	86% (1000)	[37]
Ni-Co hydroxide	nanocomposite	Electrochemical deposition	853.7	85% (1000)	[38]
Ni-Co hydroxide	nanosheets	Electrochemical applications	1725	88% (3000)	[39]
Ni(OH) <sub>2</sub> –Co(OH) <sub>2</sub> composites	nano-discs	Hydrothermal and chemical deposition	2193	84.7% (1000)	[40]
Ni-Co layered double hydroxides	nanosheets	Electrodeposition technique	983.6	76% (5000)	[41]
Ni-Co LDHs	nanosheets	Electrodeposition	2357.5	81.8% (3000)	This work

The specific capacity performance results of several types of composite materials are listed in Table 2. Table 2 shows that the Ni-Co LDH/NF electrode material obtained in this research has a higher specific capacity than the other composite materials. The specific capacity was 2357.5 F·g<sup>-1</sup>, and a rate of 81.8% was maintained after 3000 cycles, indicating that the Ni-Co LDH nanosheets material on NF substrate is an ideal energy storage material and has potential use in high-performance supercapacitors.

In conclusion, the results demonstrate that NC-2/NF has better electrochemical performance than the other samples. Three key points can be summarized. First, NC-2/NF has a complete structure and three-dimensional nanosheets. These ultrathin nanostructures grow perpendicular to the surface of the nickel foam matrix, forming stable structures and improving the charge transport and power supply capacity. In addition, the ultrathin nanosheets provide more chemically active sites and a larger reaction contact area for redox reactions, which is conducive to the rapid transfer of ions in the electrolyte. Second, according to the XRD results, there are defects in the synthesized weak crystal materials, thus forming a porous structure, which is conducive to the electrochemical measurement of electrons and ion transfer in a redox reaction to improve the electrochemical performance of electrode materials. Third, when the NiCl<sub>2</sub>/Co(NO<sub>3</sub>)<sub>2</sub> mole ratio in the electrolyte within a certain concentration range is 2:1, the synergistic effect of Ni and Co leads to an increase in the specific capacitance of Ni-Co LDH. In addition, compared to a single element system, Ni-Co hydroxides have better performance and obvious advantages. Therefore, considering the above reasons, NC-2/NF is expected to show enhanced electrochemical performance compared to other materials.

#### 4. CONCLUSIONS

In summary, this research provides a simple synthesis route for high-performance supercapacitors to prepare transition metal hydroxides. Ultrathin nanosheets of Ni-Co LDH on the

surface of the NF matrix were successfully prepared by a controllable electrodeposition approach. The electrochemical performance of Ni-Co LDHs changed as the molar ratio of  $\text{NiCl}_2/\text{Co}(\text{NO}_3)_2$  increased from 1:1 to 5:1. When the optimized  $\text{NiCl}_2/\text{Co}(\text{NO}_3)_2$  mole ratio was 2:1, the Ni-Co LDH/NF electrode material had the highest performance. When the current density was  $1 \text{ A}\cdot\text{g}^{-1}$ , the maximum specific capacitance value was  $2357.5 \text{ F}\cdot\text{g}^{-1}$ , and it had excellent capacitance retention with 81.8% retention at  $10 \text{ A}\cdot\text{g}^{-1}$  after 3000 cycles in 2 M KOH. The ultrathin nanosheet architectures supported by NF had excellent redox reversibility, and the synergistic effects between  $\text{Ni(OH)}_2$  and  $\text{Co(OH)}_2$  were a good combination for the enhancement of the electrochemical performance of the Ni-Co LDH/NF sample. Hence, the prepared samples may be an ideal electrode material for high-performance supercapacitors.

## ACKNOWLEDGMENTS

The authors gratefully acknowledge the financial support of the National Natural Science Foundation of China (Project No. 51874154), the Key Project of Yunnan Province Science and Technology Plan of China (Project No. 2014FA024), the Specialized Research Fund for the Doctoral Program of the Ministry of Education of China (Project No. 20125314110011).

## References

1. L.L. Zhang, X.S. Zhao, *Chem. Soc. Rev.*, 38 (2009) 2520.
2. J.K. Chang, C.M. Wu, I.W. Sun, *J. Mate. Chem.*, 20 (2010) 3729.
3. G. Wang, L. Zhang, J. Zhang, *Chem. Soc. Rev.*, 41 (2012) 797.
4. Hao, Chen, Linfeng, Hu, Min, Chen, Yan, Yan, Limin, Wu, *Adv. Funct. Mater.*, 24 (2014) 934.
5. M. Sebastian, C. Nethravathi, M. Rajamathi, *Mater. Res. Bull.*, 48 (2013) 2715.
6. Y. Tao, Z. Haiyan, L. Ruiyi, L. Zaijun, L. Junkang, W. Guangli, G. Zhiquo, *Electrochim. Acta*, 111 (2013) 71.
7. Q. Meng, K. Cai, Y. Chen, L. Chen, *Nano Energy*, 36 (2017) 268.
8. K.S. Kumar, N. Choudhary, Y. Jung, J. Thomas, *ACS Energy Lett.*, 3 (2018) 482.
9. Y. He, W. Chen, X. Li, Z. Zhang, J. Fu, C. Zhao, E. Xie, *Acs Nano*, 7 (2012) 174.
10. G. Yu, L. Hu, N. Liu, H. Wang, M. Vosgueritchian, Y. Yang, Y. Cui, Z. Bao, *Nano Lett.*, 11 (2011) 4438.
11. I. Sahalianov, S.K. Singh, K. Tybrandt, M. Berggren, I. Zozoulenko, *RSC Adv.*, 9 (2019) 42498.
12. M. Li, K.Y. Ma, J.P. Cheng, D. Lv, X.B. Zhang, *J. Power Sources*, 286 (2015) 438.
13. Z. Lu, Z. Chang, W. Zhu, X. Sun, *Chem. Commun.*, 47 (2011) 9651.
14. P. Elumalai, H.N. Vasan, N. Munichandraiah, *J. Power Sources*, 93 (2001) 201.
15. X. Wang, A. Sumboja, M. Lin, J. Yan, P.S. Lee, *Nanoscale*, 4 (2012) 7266.
16. P. Naveenkumar, G. Paruthimal Kalaignan, *Composites Part B*, 173 (2019) 106864.
17. X. Yin, C. Tang, L. Zhang, Z.G. Yu, H. Gong, *Sci. Rep.*, 6 (2016) 21566.
18. W. Xing, S. Qiao, X. Wu, X. Gao, J. Zhou, S. Zhuo, S.B. Hartono, D. Hulicova-Jurcakova, *J. Power Sources*, 196 (2011) 4123.
19. J. Li, M. Wei, W. Chu, N. Wang, *Chem. Eng. J.*, 316 (2017) 277.
20. K. Ma, F. Liu, M. Zhang, X. Zhang, J.P. Cheng, *Electrochim. Acta*, 225 (2017) 425.
21. J. Cao, Q. Mei, R. Wu, W. Wang, *Electrochim. Acta*, 321 (2019) 134711.
22. S.B. Kulkarni, A.D. Jagadale, V.S. Kumbhar, R.N. Bulakhe, S.S. Joshi, C.D. Lokhande, *Int. J. Hydrogen Energy*, 38 (2013) 4046.
23. M. Pang, G. Long, S. Jiang, Y. Ji, W. Han, B. Wang, X. Liu, Y. Xi, *Electrochim. Acta*, 161 (2015) 297.

24. J.T. Kloprogge, R.L. Frost, *J. Solid State Chem.*, 146 (1999) 506.
25. J. Memon, J. Sun, D. Meng, W. Ouyang, M.A. Memon, Y. Huang, S. Yan, J. Geng, *J. Mater. Chem.*, 2 (2014) 5060.
26. M. Li, S. Xu, Y. Zhu, P. Yang, L. Wang, P.K. Chu, *J. Alloy. Compd.*, 589 (2014) 364.
27. Y.-M. Wang, D.-D. Zhao, Y.-Q. Zhao, C.-L. Xu, H.-L. Li, *RSC Adv.*, 2 (2012) 1074.
28. J. Yao, P. Xiao, Y. Zhang, M. Zhan, F. Yang, X. Meng, *J. Alloy. Compd.*, 583 (2014) 366.
29. V. Gupta, S. Gupta, N. Miura, *J. Power Sources*, 175 (2008) 680.
30. S. Wang, Z. Wang, Y. Wang, J. Chen, Z. Chen, Y. Chen, J. Fu, *Green Chem.*, 21 (2019) 5960.
31. Z. Yu, Z. Cheng, S. Majid, Z. Tai, X. Wang, S. Dou, *Chem. Commun.*, 51 (2015) 1689.
32. Z. Lv, Q. Zhong, Z. Zhao, Y. Bu, *J. Mater. Sci.*, 28 (2017) 18064.
33. Y.Y. Liang, S.J. Bao, H.L. Li, *J. Solid State Electrochem.*, 11 (2007) 571.
34. M.-S. Wu, C.-Y. Huang, K.-H. Lin, *J. Power Sources*, 186 (2009) 557.
35. J. Xu, J. Wu, L. Luo, X. Chen, H. Qin, V. Dravid, S. Mi, C. Jia, *J. Power Sources*, 274 (2015) 816.
36. Y.-C. Liu, J.A. Koza, J.A. Switzer, *Electrochim. Acta*, 140 (2014) 359.
37. J. Pu, Y. Tong, S. Wang, E. Sheng, Z. Wang, *J. Power Sources*, 250 (2014) 250.
38. L. Jiang, Y. Sui, J. Qi, Y. Chang, Y. He, F. Wei, Q. Meng, Z. Sun, *Micro & Nano Lett.*, 11 (2016) 838.
39. X. Wang, T. Song, *New J. Chem.*, 40 (2016) 8006.
40. J. Li, M. Yang, J. Wei, Z. Zhou, *Nanoscale*, 4 (2012) 4498.
41. H. Li, F. Musharavati, E. Zalenezhad, X. Chen, K.N. Hui, K.S. Hui, *Electrochim. Acta*, 261 (2018) 178.